

Available online at www.sciencedirect.com

ScienceDirect

journal homepage: www.elsevier.com/locate/he

Large-scale single-step synthesis of wrinkled N–S doped 3D graphene like nanosheets from Tender palm shoots for high energy density supercapacitors

Sandhya Rani Mangiseti^a, M. Kamaraj^b, Ramaprabhu Sundara^{a,*}

^a Alternative Energy and Nanotechnology Laboratory, Department of Physics, Indian Institute of Technology Madras, Chennai, 600036, India

^b Department of Metallurgical and Materials Engineering, Indian Institute of Technology Madras, Chennai, 600036, India

HIGHLIGHTS

- Novel self N–S co-doped 3D wrinkled graphene like nanosheets (3D H-GNS) are developed from biomass Tender palm shoots.
- As-prepared 3D H-GNS exhibit high specific surface area and unique porous morphology.
- High specific capacitance of 529 F g⁻¹ at 1.5 A g⁻¹ and excellent energy density of 106.3 Wh kg⁻¹ in organic electrolyte is achieved.
- Fabricated fully bio-compatible solid-state flexible supercapacitor presents electrochemical stability up to 2000 bending angles.

GRAPHICAL ABSTRACT



ARTICLE INFO

Article history:

Received 27 May 2019

Received in revised form

6 September 2020

Accepted 21 September 2020

Available online 13 October 2020

Keywords:

Supercapacitor

Energy density

ABSTRACT

Herein, we present a simple, large-scale and low-cost process to develop hierarchically porous N–S co-doped 3D wrinkled graphene like nanosheets (3D H-GNS) from carbonization of biomass Tender palm shoots and NaHCO₃. Non-corrosive and non-toxic Na₂CO₃ acts as a reaction mean to control the activation process, developing 3D H-GNS with a high specific surface area of 2095 m² g⁻¹. A 3D H-GNS-900 electrode exhibits a high specific capacitance of 529 F g⁻¹ (1.5 A g⁻¹) and 330 F g⁻¹ (1 A g⁻¹) in 1 M H₂SO₄ for 3-electrode and 2-electrode systems respectively. Further, a longer cycle life with 93% capacitance retention over 10,000 cycles at 5 A g⁻¹ is realized. Also, we are successful in fabricating biocompatible solid-state flexible supercapacitor device with 3D H-GNS-900 electrodes in organic

* Corresponding author.

E-mail address: ramp@iitm.ac.in (R. Sundara).

<https://doi.org/10.1016/j.ijhydene.2020.09.161>

0360-3199/© 2020 Hydrogen Energy Publications LLC. Published by Elsevier Ltd. All rights reserved.

Wrinkled graphene
Nanosheets
High surface area
Biomass

electrolyte with 3 V voltage range, demonstrating to run a toy fan and lightning a LED for 15 min after charging for 60 s.

© 2020 Hydrogen Energy Publications LLC. Published by Elsevier Ltd. All rights reserved.

Introduction

Electrochemical supercapacitors store energy by charge accumulation at the electrode-electrolyte interface through non-faradaic process, which provides high power density and long cycle life as converse to batteries, where charge storage takes place due to electrochemical reduction-oxidation (red-ox) reactions. Supercapacitors find their use in high power applications like drilling, camera flash, hybrid electric vehicles and memory backup systems. However, the limitation associated with supercapacitors is low energy density, which hinders their use in predominant applications [1–5]. Supercapacitors are basically of two kinds: electric double layer capacitors (EDLCs) and pseudo capacitors (PCs). In EDLC supercapacitors, non-faradaic charge transfer occurs at the electrode-electrolyte interface whereas on contrary, faradaic reactions are responsible for the charge storage in PCs. Generally, carbon-based nanomaterials (graphene, carbon nanotubes, carbon nanofibers, activated carbon and carbon aerogel etc.) possess EDLC behavior. On the other hand, additionally attached oxygen-containing groups, carboxyl groups to carbon nanomaterials, heteroatom doping (N-, S-, P- and B-) in carbon nanostructures, metal oxides (TiO₂, MnO₂, RuO₂, CuO, Fe₂O₃, NiO, Fe₃O₄ and IrO₂ etc.) and conducting polymers (polypyrrole, polyaniline etc.) contribute to pseudo capacitance and boost the supercapacitive performance. Therefore, in order to enhance the electrochemical performance including energy density without compromising with power density and cycle life of supercapacitor, it is important to design and develop carbon-based electrode materials owning good electrical conductivity, high specific surface area and proper pore size distribution with the insertion of PC material [6–8].

Though the commercialized supercapacitors are based on activated carbon, they suffer from low specific capacitance resulting from their low electrical conductivity and a large number of micro pores, which may reduce ion and charge transportation rate [9–12]. As known, carbon nanomaterials such as graphene, carbon nanotubes, carbon nanofibers and carbon nanocomposite materials are playing a promising role in energy storage applications [13–15]. Among these, two-dimensional (2D) structured graphene sheets are seeking more attention due to high electrical conductivity, excellent mechanical strength, thermal stability, chemical stability and large surface area. Apart from this, there are many reports based on 2D carbon nanomaterials such as graphene, carbon nanosheets and their composites with a three-dimensional (3D) structure, which are used as electrode materials for energy storage applications mainly batteries and supercapacitors. 3D nanomaterials play a vital role in improving the

electrochemical performance including specific capacitance, energy density, power density and cycle life of supercapacitors. Nevertheless, in 2D structures, aggregation of graphene nanosheets due to strong van der Waals forces happens and as a result, macro particles are formed and nanosheets are not accessible for the ion adsorption and charge transportation, degrading the electrochemical performance. Thus, the better replacement for 2D graphene nanosheets would be a 3D graphene nanosheets. 3D graphene nanosheets are potential alternative electrode materials for supercapacitors due to their good electrical conductivity, unique structure with interconnected pores. 3D graphene and its derivatives find applications in different sectors namely sensors, fuel cells, batteries, hydrogen production and storage, solar cells and supercapacitors. In comparison to 2D graphene, 3D graphene manifests superior surface area and porosity that advantage them in enhancing their energy storage properties. 3D graphene exhibits increased number of active sites due to their unique morphology, leading to better electrode-electrolyte interaction and hence better electrochemical properties than 2D structures [16–20]. In the second place, heteroatom doping especially N–S doping in biomass derived carbon have got considerable attention in academia and industries due to their ability to enhance the charge storage with high energy and power densities. N-doping improves the electron-transfer properties of the carbon material whereas that of S-doping improves the pseudo capacitive performance [21–24].

The precursors used for synthesizing such carbon nanomaterials involve expensive non-renewable materials and multiple preparation steps and the use of toxic chemical/gaseous reagents, which limit their large-scale production [25,26]. Therefore, emerging a low-cost and environmentally friendly method for producing large-scale carbon nanomaterials with high specific surface area and distinctive pores structure is favorable for improving the electrochemical performance. Accordingly, 3D interconnected hierarchical porous graphene like structure with thin carbon walls and heteroatom doping is considered to be a promising electrode material. Here, the thin wrinkled walls of the graphitic carbons form a 3D graphene like network and provide a high conductivity, the unique pore structure consisting of interconnected meso, micro and macro pores, improves ion and charge transportation rate and reduces the ion diffusion path length. Designing hierarchical porous carbon materials using soft and hard templates demand number of time-consuming and expensive synthesis steps. Synthesis of high surface area conductive porous carbon materials utilizing biomass-based easy and efficient techniques for high-performance supercapacitor have found extensive interest in the recent times. Typically, the inherent microstructure and

composition of the biomass influence the final product structural and morphological properties of carbon nanomaterials and their electrochemical properties. N–S co-doped porous carbons were reported recently by using thiourea, Na_2SO_3 , 1-Amino-2-thiourea and etc. [27–30]. However, most of these precursors are expensive and might release some toxic gases during the decomposition process.

The present work demonstrates a facile single-step eco-friendly synthesis process for self N–S co-doped 3D wrinkle graphene nanosheets (H-GNS) like structure with high surface areas by carbonization of biomass Tender palm shoots. For the first time, we have used Tender palm shoots as a self N–S co-doped carbon source and to further increase the heteroatom doping content, amoxicillin is used as an N–S doping agent. Tender palm shoots, rich in carbohydrates, are easily available in Asian countries and contain 1% of water, 94.1% of carbohydrates, 4% of protein, 0.5% of fat, and 1.4% of ash. Tender palm shoots and amoxicillin are carbonized at various temperatures ranging from 700 to 900 °C with NaHCO_3 to form a 3D wrinkled porous graphene like structure. Compared with the other chemical activation process, the present method based on NaHCO_3 is better and scalable, since the organic impurities developed during decomposition process can be easily removed with deionized water rinsing. To the best of our knowledge, no reports are available on Tender palm shoots derived self N–S doped 3D H-GNS for electrochemical supercapacitor applications.

Results and discussion

The overall process involved in the preparation of biomass-derived 3D H-GNS is depicted in Fig. 1. To make sure that

the developed microstructure is appropriate, we carbonized the raw Tender palm shoots at 350 °C in the nitrogen atmosphere and examined their microstructure by scanning electron microscopy (SEM). Fig. S1a shows the porous framework assembled by carbon walls in the carbonized palm shoots (see Supplementary data file). More specifically, the observed microstructure revealed a unique multilayer structure, investigated as the layers of graphitic structure. Eventually, if we could de-laminate and avoid the agglomeration of graphitic layers, a novel and largely scalable biomass-derived 3D porous graphene like nanosheets could obtain readily. Dual heteroatom doping is found to be more productive in comparison with single heteroatom doping and presents a unique set of properties due to the synergistic effects. Hence, we presented a simple single-step green synthesis process for self N–S co-doped high surface area wrinkled 3D graphene like nanosheets using Tender palm shoots and NaHCO_3 .

Carbonization process at 700 °C and 800 °C give rise to partial delamination as shown in Figs. S1b–c. For H-GNS at 900 °C as shown in SEM micrograph (Fig. 3) the wrinkled graphene like nanosheets are obtained, which comprise of interconnected graphene like sheets intertwining each other to attain 3D structure. Particularly, randomly crumpled sheets in line with one another with thick graphene layers at the edges are found which tend to contribute high graphitization in H-GNS-900. In comparison to conventional graphene nanosheets, the thin and distinctive wrinkles are significant in the as-synthesized 3D H-GNS, which might develop from the intense gasification and self-activation through the carbonization process. As seen in Fig. S1 and Fig. 3, the carbonization temperature also influences the morphology of as-prepared samples. Further investigations by transmission electron microscopy (TEM), disclosed the intertwining of the 3D structure

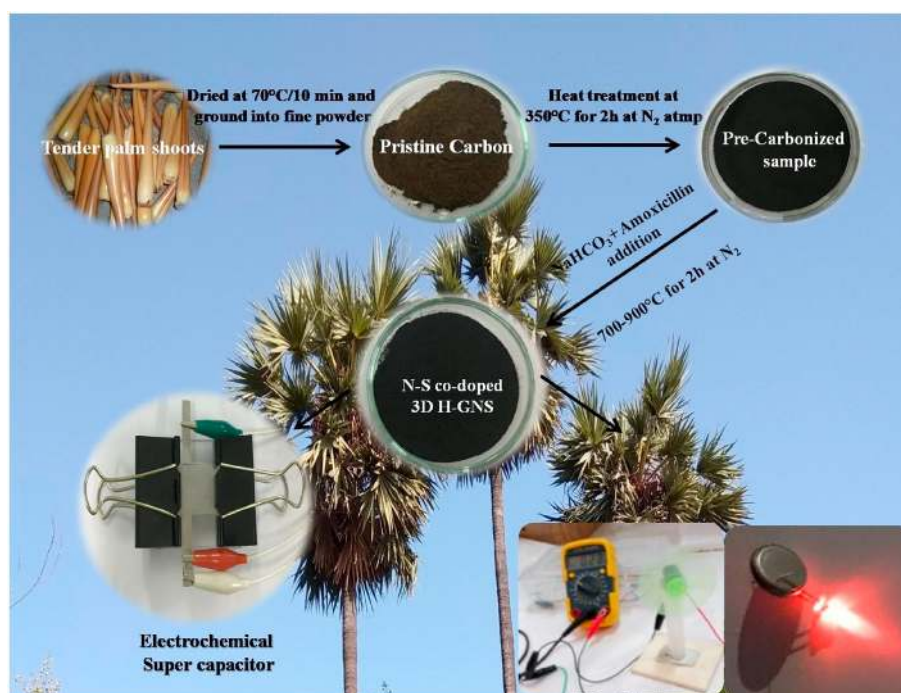


Fig. 1 – Schematic representation for the synthesis process of H-GNS from Tender palm shoots.

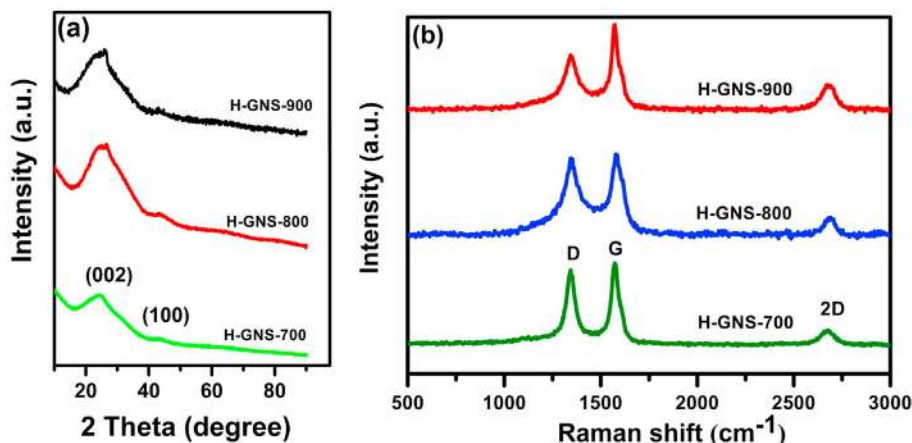


Fig. 2 – (a) X-ray diffraction patterns and (b) Raman spectra of the H-GNS-700, H-GNS-800 and H-GNS-900.

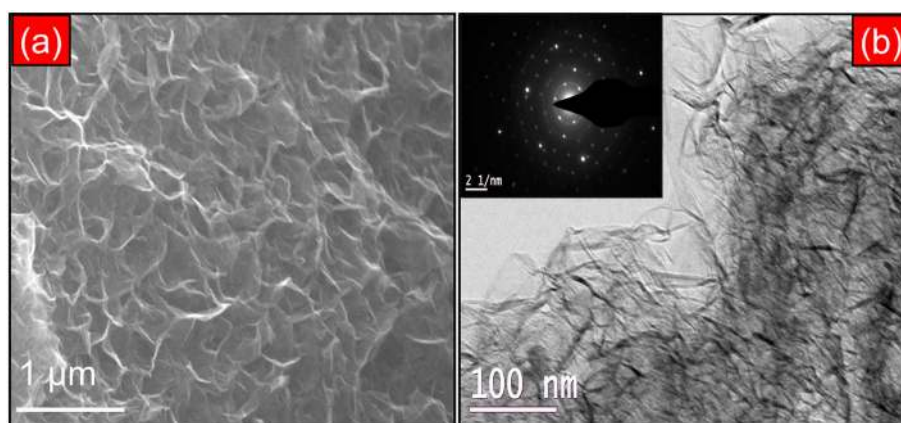


Fig. 3 – FESEM images of (a) HGNS-900 and (b) HRTEM image of the H-GNS-900 (inset shows the SAED pattern of the H-GNS-900).

resulted in thin graphene like sheets of different thickness. The TEM image depicts conventional sheets comprised of few layers of graphene like nanosheets. The selected area electron diffraction (SAED) pattern of 3D H-GNS-900 suggests explicit diffraction ring pattern, which reveals the high degree crystalline nature. The energy dispersive X-ray (EDX) elemental mapping clearly shows the homogenous distribution of nitrogen; oxygen and sulfur within the H-GNS-900 (see Fig. S3).

The graphitization degree of the prepared samples is characterized by X-ray diffraction (XRD) and Raman spectroscopy. Fig. 2a displays the characteristic XRD peaks of the samples H-GNS-700, H-GNS-800, and H-GNS-900. With the increase of carbonization temperature from 700 to 900 °C, the diffraction peak (2 0 0) slightly shifts to higher scattering angles, and there is a reduction in intensity of the weak peak at 43°, indicating the higher degree of graphitization [31]. The peaks located at 25.9° and 43° are observed after the carbonization at 900 °C, these peaks are characteristic of graphene sheets or graphene sheet like carbon materials, and indicating

a high degree of graphitization for 3D H-GNS with an interplanar spacing of 3.4 Å. The broad diffraction peak denotes the existence of wrinkled nature of graphene like nanosheets.

Further, the Raman spectra of 3D H-GNS-700-900 samples show the existence of high degree of graphitization. The peaks at 1340 cm^{-1} , 1585 cm^{-1} and 2693 cm^{-1} are related to the characteristic D (defects), G (graphitic) and 2D bands, respectively. The 3D H-GNS-900 spectrum showed a low intense D, sharp G, and 2D bands with an I_D/I_G ratio of 0.41, whereas I_D/I_G ratio for H-GNS-700 and H-GNS-800 are 0.84 and 0.89 respectively. The decreased I_D/I_G of 3D H-GNS-900 signifies relatively a higher degree of graphitization. The above results demonstrate that the spectrum is characteristic of graphene like nanosheets [32].

Then, to study the textural properties of the prepared electrode materials, nitrogen adsorption-desorption characteristics are elucidated at 77 K, and the results are presented in Fig. 4a. It is obvious that H-GNS-700 to H-GNS-900 exhibit both Type I and Type IV characteristic adsorption-desorption

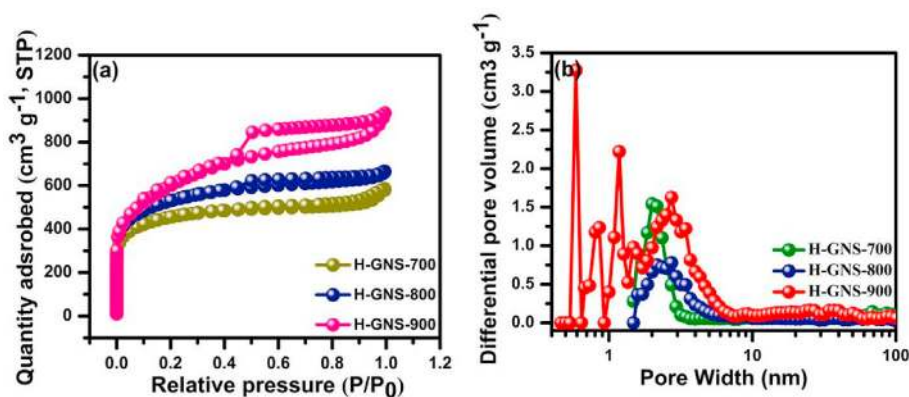


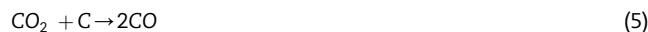
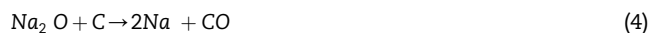
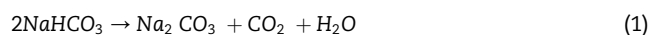
Fig. 4 – (a) Nitrogen adsorption-desorption isotherms at 77 K and (b) pore size distributions of H-GNS-700, H-GNS-800 and H-GNS-900.

isotherms, which substantiates the hierarchical porous structure of the H-GNS samples [33]. There is significant prompt rise at lower pressures, attributes the presence of the micropores, and a broad curve that extends from $P/P_0 = 0.4$ to 1 for H-GNS-700 to H-GNS-900 demonstrates the mesoporous structure. However, a significant hysteresis loop and obvious kink at high pressures ($P/P_0 > 0.4$) for H-GNS samples, signifies the development of the small number of macropores. Fig. 4b shows the pore size distribution (PSD) calculated using DFT (density functional theory) model. The specific surface area of H-GNS-900 found to be $2095 \text{ m}^2 \text{ g}^{-1}$, which is greater than that of H-GNS-700 ($1478 \text{ m}^2 \text{ g}^{-1}$) and H-GNS-800 ($1738 \text{ m}^2 \text{ g}^{-1}$). With increasing the carbonization temperature from 700 to 900 °C, the total pore volume progressively increases from $0.90 \text{ cm}^3 \text{ g}^{-1}$ for the H-GNS-700 to $1.45 \text{ cm}^3 \text{ g}^{-1}$ for the H-GNS-900. However, the pore diameter gradually decreased from 4.0 nm for the H-GNS-700 to 3.38 nm for the H-GNS-900. We can scrutinize that all the prepared electrode materials exhibit hierarchical (micro, meso and macro) pore structure. The well-developed mesopores resulted from the interaction between NaHCO_3 and Tender palm shoots.

The detailed mechanism for the synthesis of N–S co-doped high surface area 3D H-GNS is explained as below. The self N–S co-doped 3D H-GNS formed with N (2.1 at %) and S (0.45%), when the biomass and NaHCO_3 is carbonized at 700 °C. To further enhance the N–S doping amount, the combination of Tender palm shoots, NaHCO_3 and amoxicillin are used as precursors, in which Tender palm shoots acted as a carbon source, NaHCO_3 as pore-creating agent and amoxicillin as an N–S co-doping agent. When increasing the carbonization temperature from 700 to 900 °C, high surface area porous 3D H-GNS samples are developed. In addition, through the reaction with the decomposed ammonia (NH_3) and SO_3 from the amoxicillin, a fraction of carbon atoms is replaced by nitrogen and sulfur and finally high amount of N–S doped 3D H-GNS is obtained. Here, Na_2CO_3 plays a promising role in ripping off and using the sp^3 hybridized carbon atoms in between the graphitic layers of Tender palm shoots derived carbon. Once the Na_2CO_3 is decomposed, resultant Na atoms catalyzed the graphitic microstructures to form a 3D wrinkled graphene sheets like structure. Also, the

pore formation is developed by the release of CO_2 from the surfaces once NaHCO_3 is decomposed. The Na_2CO_3 is emancipated and trapped in the inner pores developed by CO_2 gas bubbling, which helps in the development of micro and mesopores. The released CO_2 further interacts with carbon through the gasification resulting in thinner walls. It is well reported that K, Na, and Ca are liable to catalyze the high graphitization of amorphous carbon and these atoms can develop charge transfer centers with aromatic hydrocarbons and also with graphitic layers to obtain crystallinity. For the presence of inherent inorganic elemental composition, see Table S1. Elements such as K, Na, Ca, P, Fe and Cl, influence the self-activation of Tender palm shoots which enhances the graphitization degree. Where, the Cl ions etch out the carbon structure and developed micro and mesopores, and K, Na and Ca prevent the generation of van der Waals force, which hinders the aggregation of sp^2 hybridized carbon layers and results in 3D graphene-like structure. In addition, while increasing the carbonization temperature, oxygen also contributes to etching the graphitic layers to develop 3D graphene like sheets.

The pore formation mechanism is explained as follows:



The existence of wrinkles offers the enhanced ion interaction at the electrode-electrolyte interface. Na_2CO_3 is a general carbon activation agent, the use of Na_2CO_3 is reported in literature as activation agent for the synthesis of porous carbon and there is no report for obtaining 3D-graphene like nanosheets structure. The possible reason could be: some of the biomass materials might react directly with Na_2CO_3

without being subjected to carbonization which would certainly generate a huge amount of tar in the reaction and this tar is possible to hinder the catalytic effect of Na_2CO_3 . The reaction temperature also plays a major role, the reordering of graphitic microcrystals is restricted at temperature below the melting point of Na_2CO_3 (850 °C). It is realized that no graphene-like sheets are developed when the carbonization is done below 900 °C. According to previous reports, few 3D graphene like materials are developed from some of the biomass precursors, but they have used multiple and critical preparation steps. Herein we have used a single preparation step for self N–S co-doped 3D graphene like sheets.

X-ray photoelectron spectroscopy (XPS) is used to understand the chemical composition of the 3D H-GNS-900. The higher resolution survey spectrum as shown in Fig. S4 confirms the presence of N, C, O and S in H-GNS-900. The high-resolution N1 spectra is deconvoluted to four different peaks, which correspond to pyridinic (N6, 398.3 eV), pyrrolic (N5, 399.9 eV), quaternary (Q_N , 400.8 eV) and oxidized-N (N-Ox, 402.4 eV) [34,35]. Typically, pyrrolic N and pyridinic N are located along the wings of the graphitic carbon plane, while the quaternary N are located at the wings of graphitic carbon plane and within the oxidized 3D graphene like sheets. It is well known that the insertion of even small amounts of heteroatoms (N, S) can significantly improve the physicochemical properties of the carbon network, such as electrochemical activity, conductivity and oxidation stability. In aqueous electrolyte, it is believed that both pyrrolic N and pyridinic N are electrochemically active, which offers the extra pseudo capacitance, whereas the inserted quaternary N into the graphitic planes bonded to the three carbon atoms contribute to the electron transfer and significantly improve the electrical conductivity of carbon network. The deconvoluted S 2p spectra have peaks at 164.0 eV, 165.5 eV, 167.9 eV and 169.3 eV, respectively. The initial two dominated peaks correspond to the S 2p_{3/2} and S 2p_{1/2} peaks for the thiophene-S (-C-S-C) due to a spin-orbit coupling, which contributes the pseudo capacitance behavior, and the peaks at 167.9 and 169.3 eV correspond to the oxidized sulfur group C-SO_x-C. The obvious development of volatile S–O groups could be responsible for the relatively reduced percentage of S in the prepared samples compared to N after carbonization. The C1s peak at 284.5 eV, 285.8 eV, and 286.8 eV corresponds to sp² hybridized C(C=C) atoms in graphene, a broad high-intensity shoulder peak relates to sp²-C atoms bonded to S and carbonyl groups such as (C=C), (O–C–O) and a low-intensity sp³ C–N bonds, respectively. The peak at 531.1 eV (C=O) in the O1s spectra shows the existence of oxygen atoms, which efficiently participate in contributing to the pseudo capacitance by improving the wettability of carbon material and involves in faradaic reactions. Elemental composition of prepared materials at different temperatures are determined by XPS and the composition values are listed in Table S2.

Electrochemical performance of N–S co-doped 3D wrinkled graphene sheets-based carbon electrodes

The electrochemical performances of H-GNS 700–900 electrode materials are examined in the aqueous 1 M H₂SO₄ electrolyte. Fig. S5a represents the cyclic voltammetry (CV)

curves for H-GNS-700 and H-GNS-800 with the nearly rectangular shape at the scan rate of 100 mV s⁻¹. The specific capacitance (C_p) of H-GNS-700 and H-GNS-800 electrodes is measured from the charge-discharge (CD) profiles as shown in Fig. S5b at 1 A g⁻¹. CD curves present the non-linear shape, which indicates both EDLC and PC nature and exhibit capacitance of 270 F g⁻¹ and 364 F g⁻¹ for H-GNS-700 and H-GNS-800 electrodes, respectively.

In order to observe the stability of prepared electrode material, we have done the electrochemical testing of H-GNS-900 in various electrolytes, both in three- and two-electrode configurations at various scan rates and current densities. Initially, the performance of the H-GNS-900 electrode is examined in a three-electrode configuration using 1 M H₂SO₄. Fig. 5a shows the CV profiles of H-GNS-900 in a potential window of 0–1 V. It shows a quasi-rectangular shape at various scan rates with slight pseudo capacitive contribution due to the influence of surface heteroatom (N, S) functionalities. Further electrochemical performance is studied with the CD profiles at different current densities as shown in Fig. 5b. It exhibits the nonlinear behavior with the high charge-discharge rate. A high specific capacitance of 529 F g⁻¹ is obtained at 1.5 A g⁻¹ current density. The increase in current density from 1.5 to 3, 6, 8 and 30 A g⁻¹ results in a gradual decrease in specific capacitance from 529 to 424.8, 420, 377.6, 347.5 F g⁻¹, respectively. A specific capacitance of 347.5 F g⁻¹ is still sustained even at a high current density of 30 A g⁻¹, which further proves the high ion transfer rate i.e. good rate capability of H-GNS.

Compared with the earlier reports, it is worthy to note that a specific surface area value does not certainly promote a high specific capacitance. For example, while the excellent surface area (2557 m² g⁻¹) of the carbon derived from silk fibroin displayed a specific capacitance of 264 F g⁻¹; the much lower surface area (221 m² g⁻¹) of the activated carbon obtained from eggshell membrane exhibited a high specific capacitance of 297 F g⁻¹. The huge variation can be principally ascribed to the variation in their specific active surface area, which can be greatly progressed by a unique morphological structure, such as in case of carbon derived from the eggshell. Thus, a suitable morphological structure can promote a high specific active surface area (accessible surface area for electrolyte ion interaction). This is quite persistent with our data, where the substantially high specific capacitance (529 F g⁻¹) with an adequate surface area (2095 m² g⁻¹) apparently signifies the high active specific surface area of the 3D H-GNS-900. Here, the excellent electrochemical performance of H-GNS-900 is due to the 3D wrinkled graphene like sheets with interconnected pore structures, which not only exhibits the high specific surface area but also shortens the ion diffusion path length and assists the quick ion transportation. Furthermore, the doping with heteroatoms offers high electrical conductivity, pseudo capacitance and hence better performance.

To further investigate the electrochemical performance of H-GNS-900, a symmetric supercapacitor is fabricated using 1 M H₂SO₄. From Fig. 5c, CV curves show rectangular shape, this is maintained even at high scan rates, denoting the ideal capacitive behavior and good rate performance. In addition, the CD profiles display the symmetrical triangular shape even at higher current densities with no remarkable IR drop; specify

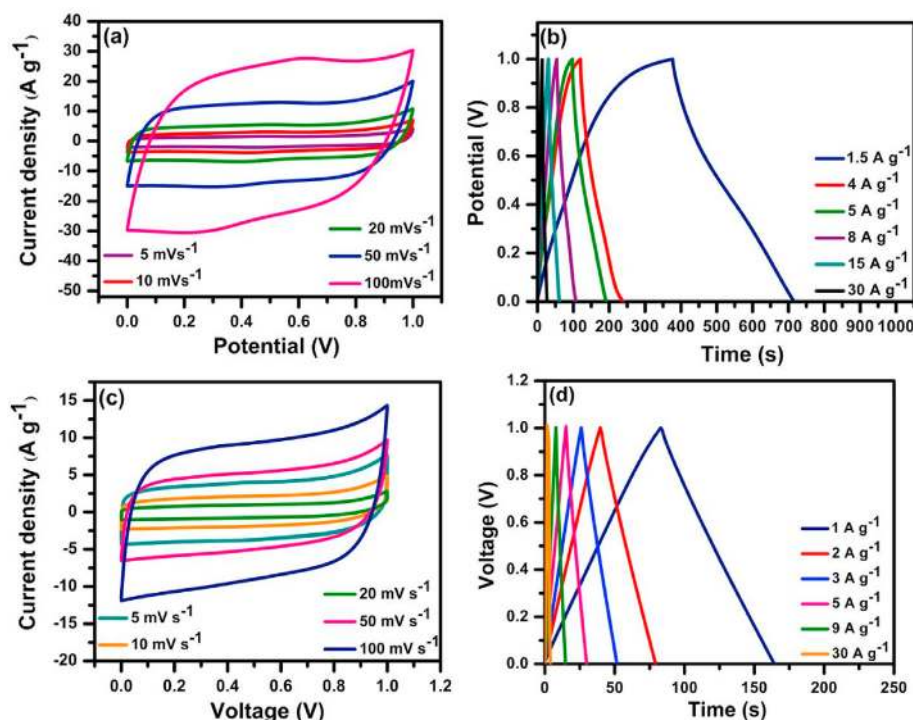


Fig. 5 – Electrochemical capacitive behavior of the H-GNS-900 measured in a three-electrode system: (a) CV curves, and (b) GCD curves in 1 M H₂SO₄; (c) CV curves, and (d) GCD curves in 1 M H₂SO₄ for two electrode configurations.

the electrochemical reversibility with low internal resistance (Fig. 5d). A high specific capacitance of 330 F g⁻¹ at 1 A g⁻¹ and a gradual decrease in specific capacitance (148 F g⁻¹) is observed with increased current density (30 A g⁻¹). The symmetric system also exhibits a maximum energy density of 11.5 Wh kg⁻¹ at a power density of 0.5 kW kg⁻¹. Information on variation of N, S content with carbonization temperature and its influence on electrochemical performance is given in the supplementary data file.

Further, a standard technique to study equivalent series resistance (R_s), charge transfer resistance (R_{ct}), and capacitive behavior etc. widely known as electrochemical impedance spectroscopy (EIS) is implemented. The Nyquist plot of H-GNS-900 electrode in 1 M H₂SO₄ in the frequency ranges from 100 kHz to 10 mHz is shown in Fig. S6. A semicircle at high frequencies with a diameter of ~2.89 Ω along the real axis denotes the charge-transfer resistance at the electrode-electrolyte interface. This low R_{ct} could be due to the unique 3D porous graphene sheets with the interconnected hierarchical porous structure, which reduces the ion diffusion length, acts as ion transportation channels and also behave as ion buffering reservoirs. The low equivalent series resistance of ~0.28 Ω, at a high-frequency region, signifies that the hetero-atom doping increases pore accessibility for the ions, and are facilitated with good intrinsic electronic properties of the electrode material, also it could be due to the smaller contact resistance between the electrode material and electrolyte ions. The vertical line at mid-frequency range is a characteristic of ideal capacitor behavior denotes the Warburg

impedance ascribed to the frequency dependence of ion diffusion/transfer. In addition, the wrinkled thinner walls of the H-GNS-900 improve the diffusion of the ions readily. The measured values from the Nyquist and bode plot are given as below; $R_s = 0.28 \Omega$, $R_{ct} = 2.89 \Omega$, $W = 0.47 \Omega$. From the bode plot, it is observed that the phase angle of H-GNS is 88° which is nearer to that of an ideal capacitor value of 90°. This resulting of low equivalent series resistance, low charge-transfer resistance, low relaxation time, high phase angle and excellent specific capacitance suggest the superior electrochemical properties of H-GNS, which are favorable for a supercapacitor device. The variation of the phase angle from 90° supports the pseudo capacitive behavior. Relaxation time constant ($\tau_0 = 1/f_0$, $f_0 = \text{frequency at } -45^\circ$) is a significant feature of the supercapacitor device. Time constant for H-GNS is found to be 2.1 s. This low relaxation time of H-GNS reveals diffusion of ions deeper into the electrode material and that the supercapacitor device achieved its maximum capacitance with rapid recharging. It is well recognized that the high-power density relates to lower relaxation time constant values. This value is rapid than that of the commercially available Maxwell's supercapacitors (3.86 s).

In the present scenario, flexible supercapacitors are given considerable attention in flexible energy storage device for wearable applications such as electronic appliances, electric devices and smart garments etc. Considering the notable role of electrolyte and current collectors in such design, we intent to assemble solid-state flexible supercapacitor using H-GNS-900 as an electrode material with PVA/H₂SO₄ based solid-state

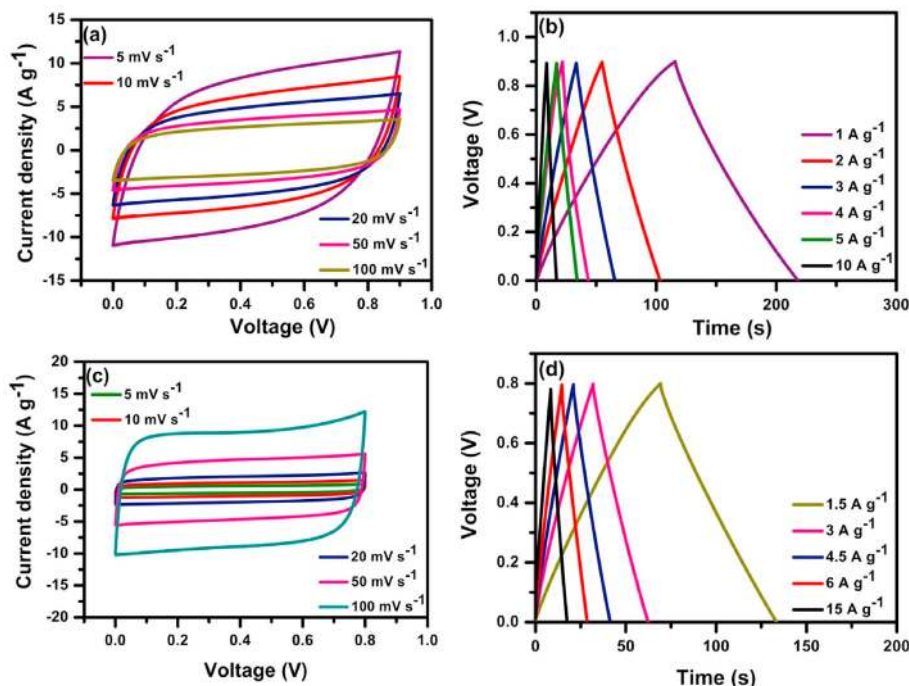


Fig. 6 – Electrochemical studies of H-GNS-900 (a) CV curves in PVA/H₂SO₄ gel electrolyte, (b) GCD curves in PVA/H₂SO₄; (c) CV curves in Agarose/NaCl hydrogel electrolyte, (d) GCD profiles in Agarose/NaCl in two electrode configurations.

gel electrolyte. The CV and CD performance of such fabricated device is shown in Fig. 6a–b. The CV curves show nearly rectangular shape in the potential window of 0–0.9 V, and the measured specific capacitance from the CD curves is 112.1 F g⁻¹ at 1 A g⁻¹. The step by step decrement in specific capacitance 105.7, 104.3, 94.6, 93.3, 91.11 F g⁻¹ is observed as the current density is increased. It retains 81.3% of initial capacitance and exhibits high energy of 12.6 Wh kg⁻¹ at a power density of 450 W kg⁻¹, respectively.

Further, we report a fully bio-compatible solid-state flexible supercapacitor using a NaCl-Agarose hydrogel electrolyte. It is less expensive and environmentally friendly, consists of chemically interconnected Agarose backbone with sub micrometer pores. NaCl-Agarose gel electrolyte is prepared by inclusion of both Na⁺ and Cl⁻ ions into hydrogen-bonded interconnected self-construction of molecules of Agarose gel. This porous structured gel electrolyte facilitates the rapid ion transfer channels, resulting in high-energy storage capacity. To all above, the simple gelation process, low cost of Agarose and NaCl salt, permits this solid-state flexible supercapacitor to be fabricated appreciably. Fig. 6c shows the CV curve for biocompatible solid-state flexible supercapacitor. It reveals a quasi-rectangular shape at different scan rates and C_p is measured from the CD curves (Fig. 6d) at current densities in the range of 1.5–15 A g⁻¹. CV plots demonstrate symmetrical shape with a small IR drop in a wide range of current densities signifying excellent rate capability. A C_p of 120 F g⁻¹ at 1.5 A g⁻¹ and a C_p of 95 F g⁻¹ is still maintained at a high current density of 15 A g⁻¹. It also shows high rate capability of 79% at a current density of 15 A g⁻¹ with a high

energy density of 10.6 W h kg⁻¹ and power density of 599 W kg⁻¹. Calculations are made based on considering total mass of the two symmetric electrodes. There are no observed changes in CD curves when flexible capacitor is bended at angles from 0 to 180° at a current density of 1.5 A g⁻¹ as shown in Fig. S7a. Interestingly, the three flexible supercapacitors connected in series can power up a red LED for 15 min after charging for 60 s.

The commercial supercapacitor industry is dominated by organic electrolyte owing to their high working voltage range. Also, it facilitates the utilization of cheaper materials for current collectors and packages. In this work, 1.5 M tetraethylammoniumtetrafluoroborate (TEABF₄) in PC solution is used as electrolyte. The CV and CD profiles are shown in Fig. 7a–b in an organic electrolyte. The H-GNS-900 exhibits a superior C_p of 140, 132, 124, 109 F g⁻¹ at 1, 2, 5, and 10 A g⁻¹ current density respectively and also presents a high energy density of 43.75 Wh kg⁻¹ at a power density of 750 W kg⁻¹. Comparison of electrochemical performance of the present work with previously reported biomass-derived porous carbon listed in Table S3. Noticeably, the calculated specific capacitance for H-GNS-900 in the organic electrolyte is lower than that of aqueous electrolyte, attributed to the larger solvated ion sizes and lower dielectric constants of organic electrolytes. Also, the pseudo capacitance contribution from carbon-based electrode materials is less in case of organic electrolytes.

Furthermore, non-aqueous electrolytes such as ionic liquids are acquiring the potential interest in energy storage devices due to their high and stable voltage range. Added to

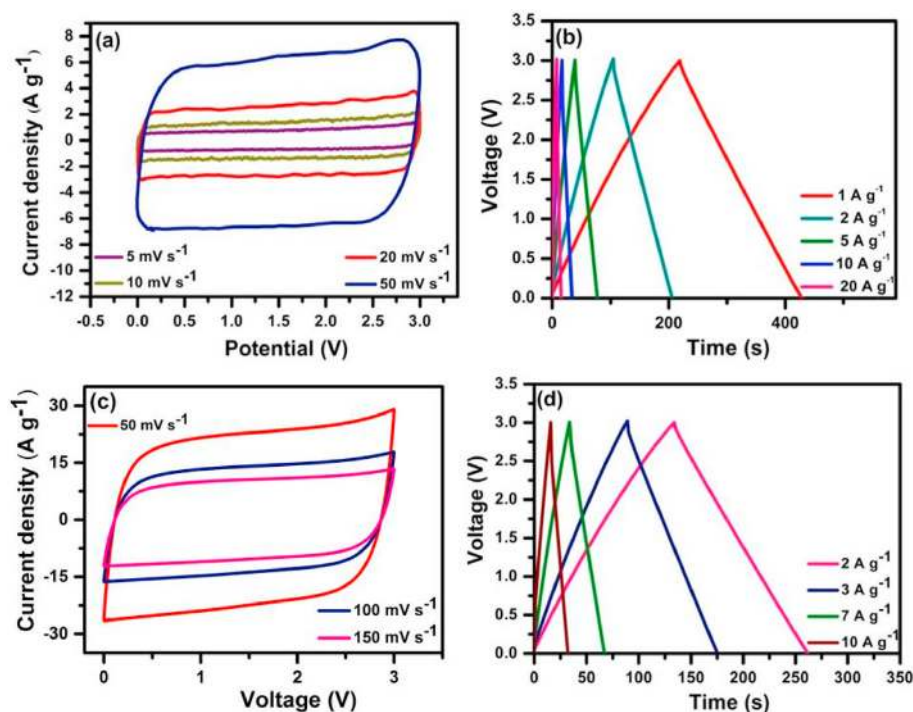


Fig. 7 – Electrochemical performance characteristics measured in two electrode configuration (a) CV curves at various scan rates, and (b) GCD curves at different current densities in 1.5 M TEABF₄/PC electrolyte; (c) CV curves of H-GNS/IL, (d) CD profiles at various current densities in [BMIM][TFSI] electrolyte.

the above, high ionic conductivity, a wide voltage window (3–7 V), low vapor pressure, superior thermal and electrochemical stability make ionic liquids an ideal eco-friendly alternative to organic electrolytes. However, the presence of water molecules may reduce the working potential of ionic liquids. Hence, to overcome this, we have used hydrophobic 1-butyl-3-methylimidazolium bis (trifluoromethanesulfonyl) imide [BMIM][TFSI] ionic liquid at atmospheric conditions to obtain high energy and power densities. In general, ionic liquid-based supercapacitors are fabricated in glove box condition but in the present work, we have assembled the symmetric device using environmentally compatible [BMIM][TFSI] ionic liquid. The CV curve and CD plots of H-GNS-900 electrode in [BMIM][TFSI] are shown in Fig. 7c–d. The curves have the nearly rectangular pattern, and stable up to working voltage of 3 V. A specific capacitance of 85 F g⁻¹ at 2 A g⁻¹ is realized for the full device and this value is comparably high to the reported values. This advancement in the working potential and the specific capacitance in ionic liquid electrolyte resulted in enhanced energy and power density of 106.3 Wh kg⁻¹ and 3 kW kg⁻¹ respectively. This enhanced electrochemical performance in ionic liquid electrolyte can be attributed to (i) the high specific surface area and unique pore size distribution which matches the size of the electrolyte ion leading to substantial specific capacitance improvement; (ii) the interaction of lone pair electrons in nitrogen atoms of H-GNS and imidazolium ring which greatly improves the binding energy, charge transfer from nitrogen to carbon atoms, thereby enhanced electrical conductivity leading to improved

performance; (iii) the unique pore nature and the large amount of wrinkles present in the surface of H-GNS increases the surface accessibility to ions, decrease the electrolyte ion diffusion distance to the inner pore walls thereby contributing more to improved electrochemical performance.

Fig. 8a displays the Ragone plots of the H-GNS-900, i.e., the energy densities versus power densities, determined in various electrolytes. Impressively, excellent energy density of 106.3 Wh kg⁻¹ at a power density of 3 kW kg⁻¹ in the ionic liquid, and large energy density of 43.75 Wh kg⁻¹ at a power density of 750 W kg⁻¹ in an organic electrolyte is achieved. This realized energy and power densities in organic and ionic liquid electrolytes are higher than the previous reports on heteroatom doped carbon materials derived from biomass. The long-term stability of electrode materials is a crucial parameter for their potential applications in practical supercapacitors. Fig. 8b shows the rate capability plot in various electrolytes. In addition, the cyclic capability of H-GNS-900 electrode is studied for continuous 10,000 cycles (see Fig. 8c) at 5 A g⁻¹ current density and surprisingly 93% of initial capacitance is retained over 10,000 cycles. The above observation validates that the Tender palm shoots derived carbon holds excellent electrochemical stability and good electrochemical performance in the three, and two-electrode systems. Due to high power/energy density, H-GNS based supercapacitor could power up a red LED with 3 V voltage window in the organic electrolyte and drive a toy fan. The energy density levels with recent reports are compared in the Ragone plot with our work [36–47].

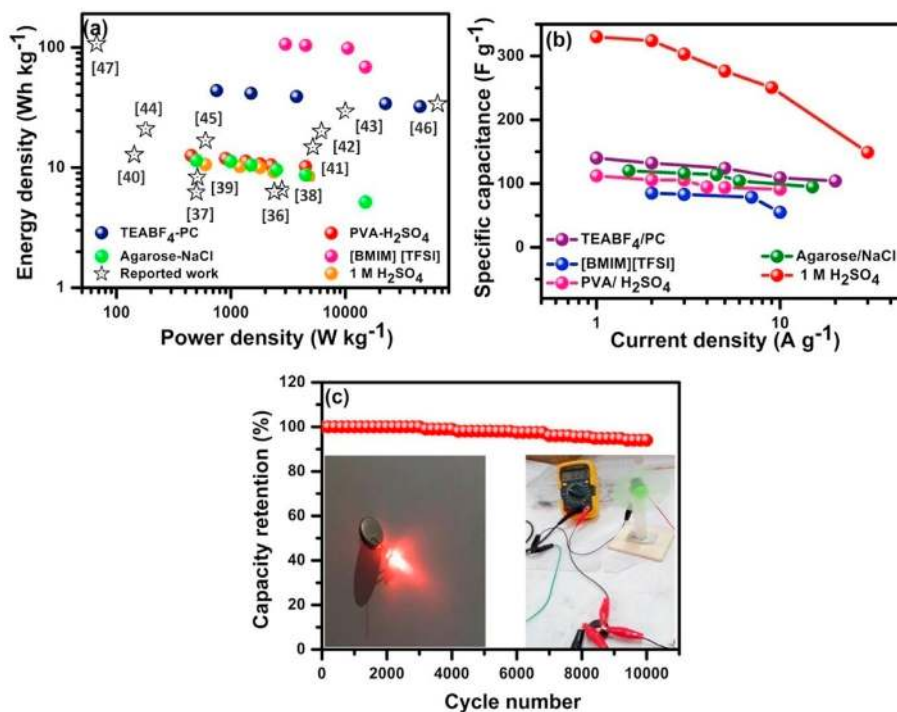


Fig. 8 – (a) A Ragone plot; (b) Specific capacitance as a function of current densities in different electrolytes for H-GNS-900; (c) Capacitance retention of H-GNS-900 at a current density of 5 A g⁻¹ over 10,000 cycles in 1 M H₂SO₄.

Conclusion

In conclusion, self N–S co-doped hierarchical porous 3D graphene like nanosheets are developed through a simple carbonization and self-activation process from biomass Tender palm shoots. The inherent inorganic elements composition such as K, Cl, P, O, S, Ca and Fe in biomass influence a self-activation in addition to the carbonization process in presence of Na₂CO₃ and thereby produce a unique porous wrinkled 3D graphene-nanosheets. Moreover, H-GNS-900 electrode material exhibits a high electrochemical performance in various aqueous and non-aqueous electrolytes. This is due to the high specific surface, hierarchical 3D porous structure, the high degree of graphitization, and excellent electrical conductivity along with nitrogen-sulfur co-doping. The present results suggest the possibility of utilizing nature to improve the development of electrode materials with high performance through simple methods. This method holds significance for the low-cost and large-scale production of excellent performance electrode materials for electrochemical devices.

Experimental

Materials synthesis

In a typical preparation process, the Tender palm shoots is dried in air and ground to a fine powder. The obtained fine powder is pre-carbonized at 350 °C for 2 h under N₂ gas flow in

a tubular furnace, which resulted in the complete decomposition of carbohydrates to carbon. The collected pre-carbonized sample is mixed with NaHCO₃ in 1:1 mass ratio. The entire mixture is dissolved in DI water, kept undisturbed for overnight, later the mixture dried at 70 °C for 8 h. The dried sample is then placed in a ceramic crucible and heated at 700 °C for 2 h under N₂ atmosphere. To further enhance the N–S co-doping amount the above procedure is repeated with the addition of 15 wt % of Amoxicillin followed by carbonization from 700 to 900 °C (heating rate 5 °C per minute) for 2 h, under N₂ gas flow in a tubular furnace. The collected sample is washed with ethanol and de-ionized water to remove the impurities such as Na₂CO₃. Finally, the 3D H-GNS sample is collected by drying at 80 °C overnight in an oven. The obtained samples are referred as H-GNS-700, H-GNS-800 and H-GNS-900.

Materials characterization

The structural properties of prepared materials were analyzed by using X-ray diffraction (XRD) studies conducted with a PANalytical X'Pert Pro X-ray diffractometer with a CuK α radiation source ($\lambda = 0.15406$ nm) in the 2θ range between 5° and 90° with a step size of 0.02. Raman spectroscopy measurements were taken using a confocal WiTech Raman spectrometer with an Nd: YAG laser (532 nm). For morphological studies, FEI Inspect F scanning electron microscope was used. The morphology of the samples was observed using high-resolution transmission electron microscopy (HR-TEM) with

a Tecnai G2 20 operated at 200 keV. The surface chemical characteristics were performed by energy dispersive spectroscopy (EDX). Surface area and pore size distribution analysis of H-GNS were performed in micromeritics ASAP 2020 instrument. X-ray photoelectron spectroscopy was carried out in Specs X-ray photoelectron spectrometer, X-ray source being Mg K α and analyzer PHOIBOS 100MCD.

Electrochemical characterization

The working electrodes are prepared by mixing 80 wt % as-synthesized powder samples with 15 wt % acetylene black and 5 wt % Polytetrafluoroethylene (PTFE). After that, N-Methyl-2-pyrrolidone (NMP) is added to form homogenous slurry, which is coated on a piece of a carbon sheet current collector. The loading of as-prepared sample on carbon sheet is approximately 2 mg with an area of 1 cm². The as-prepared electrodes are dried at 70 °C overnight. The electrochemical measurements (Cyclic voltammetry (CV), charge-discharge (CD) characteristics and electrochemical impedance spectroscopy (EIS) measurements) are carried out on a CH1608C workstation. The electrochemical response of 3D H-GNS is studied in three and two electrode configurations in aqueous (1 M H₂SO₄) electrolyte. For the three-electrode system, 3D H-GNS, Ag/AgCl, and Pt wire are used as working, reference and counter electrodes, respectively. The EIS measurement is conducted for the 3D H-GNS electrode material in the frequency ranging from 10 mHz to 100 kHz with 5 mV amplitude. In order to practically exhibit the potential applications of H-GNS in supercapacitors, the model supercapacitor device is assembled in ionic liquid [BMIM] [TFSI], all solid-state gel electrolyte (PVA/1 M H₂SO₄), NaCl-Agarose hydrogel and with organic electrolyte (TEABF₄/PC). The supercapacitor assembly consists of H-GNS-900 coated carbon sheet as electrodes, polypropylene membrane as a separator, [BMIM] [TFSI] ionic liquid as an electrolyte and stainless sheets (SS) as current collectors. A separator soaked and dried with ionic liquid is placed between two electrodes. This setup is further sandwiched between two Perspex sheets along with SS current collectors. Similarly, all-solid-state supercapacitor device is fabricated using gel electrolyte (PVA/1 M H₂SO₄) placed between the electrode materials coated on carbon cloth. The specific capacitance (C), power density (P), and energy density (E) values are measured using the below-given equations. For two electrode system in the organic electrolyte, H-GNS-900 material slurry is prepared, coated on aluminum foil, dried initially at 60 °C for 12 h and later at 120 °C for 6 h. The prepared electrodes are then cut into 12 mm discs and used for coin cell fabrication. The cell is constructed in a glove-box under an argon atmosphere using 2032-type coin cell, glassy fiber (GF/D) from Whatman as a separator and 1.5 M tetraethylammoniumtetrafluoroborate (TEABF₄) in PC solution as electrolyte. Agarose-NaCl bio-compatible gel electrolyte is prepared by addition of 1 g of Agarose powder to 0.5 M NaCl solution followed by continuous magnetic stirring, and simultaneous heat treatment at 100 °C. The resultant agarose gel is poured on a glass plate and allowed to cool down at room temperature. As prepared thick gel film was removed from the glass plate, and then sandwiched with H-GNS-900 electrodes.

For three electrode configurations [48,49]

$$C = \frac{I}{m \times \frac{\Delta E}{\Delta t}} \quad (7)$$

For the two electrode configuration [50–52]

$$C = \frac{4 \times I}{m_1 \times \frac{\Delta E}{\Delta t}}; \text{ specific capacitance of the single electrode of full cell} \quad (8)$$

$$C = \frac{I}{M \times \frac{\Delta E}{\Delta t}}; \text{ for full device specific capacitance} \quad (9)$$

$$E = \frac{1 \times C \times (\Delta E)^2}{2 \times 3.6} \quad (10)$$

$$P = \frac{E \times 3600}{\Delta t} \quad (11)$$

where C stands for the specific capacitance, I is the discharge current, ΔV is the working potential of the electrode material, Δt is the discharge time, m is the mass of the active material on electrodes, m₁ is the mass of the active material on two electrodes, M is the total active mass of the two electrodes, E is the energy density and P is the power density of the full device.

Declaration of competing interest

The authors declare that they have no known competing financial interests or personal relationships that could have appeared to influence the work reported in this paper.

Acknowledgment

The authors thank Indian Institute of Technology Madras (IITM), India and Ministry of Human Resources and Development (MHRD), Government of India for financial support. Authors would also like to thank Mr. K Nanaji (ARCI) for his assistance in executing electrochemical measurements in organic electrolyte. We thank Sophisticated Analytical Instruments Facility (SAIF), IITM, Chennai, for providing essential instrumental facility.

Appendix A. Supplementary data

Supplementary data to this article can be found online at <https://doi.org/10.1016/j.ijhydene.2020.09.161>.

REFERENCES

- [1] Mei L, Cui X, Duan Q, Li Y, Lv X, Wang H guo. Metal phthalocyanine-linked conjugated microporous polymer hybridized with carbon nanotubes as a high-performance flexible electrode for supercapacitors. *Int J Hydrogen Energy*

- 2020;45:22950–8. <https://doi.org/10.1016/j.ijhydene.2020.06.208>.
- [2] Zhu X, Tao H, Li M. Co-precipitation synthesis of nickel cobalt hexacyanoferrate for binder-free high-performance supercapacitor electrodes. *Int J Hydrogen Energy* 2020;45:14452–60. <https://doi.org/10.1016/j.ijhydene.2020.02.188>.
- [3] Wazir MB, Daud M, Ullah N, Hai A, Muhammad A, Younas M, et al. Synergistic properties of molybdenum disulfide (MoS₂) with electro-active materials for high-performance supercapacitors. *Int J Hydrogen Energy* 2019;44:17470–92. <https://doi.org/10.1016/j.ijhydene.2019.04.265>.
- [4] Mangiseti SR, Pari B, Kamaraj M, Ramaprabhu S. Performance of partially exfoliated nitrogen-doped carbon nanotubes wrapped with hierarchical porous carbon in electrolytes. *ChemSusChem* 2018;11:1664–77. <https://doi.org/10.1002/cssc.201800147>.
- [5] Liu L, Niu Z, Chen J. Unconventional supercapacitors from nanocarbon-based electrode materials to device configurations. *Chem Soc Rev* 2016;45:4340–63. <https://doi.org/10.1039/c6cs00041j>.
- [6] Sowmya Selvakumar M. Multilayered electrode materials based on polyaniline/activated carbon composites for supercapacitor applications. *Int J Hydrogen Energy* 2018;43:4067–80. <https://doi.org/10.1016/j.ijhydene.2017.10.106>.
- [7] Demir M, Ashourirad B, Mugumya JH, Saraswat SK, El-Kaderi HM, Gupta RB. Nitrogen and oxygen dual-doped porous carbons prepared from pea protein as electrode materials for high performance supercapacitors. *Int J Hydrogen Energy* 2018;43:18549–58. <https://doi.org/10.1016/j.ijhydene.2018.03.220>.
- [8] Lal MS, Arjunan A, Balasubramanian V, Sundara R. Redox-active polymer hydrogel electrolyte in biowaste-derived microporous carbon-based high capacitance and energy density ultracapacitors. *J Electroanal Chem* 2020;870:114236–44. <https://doi.org/10.1016/j.jelechem.2020.114236>.
- [9] Mangiseti SR, Kamaraj M, Sundara R. Green approach for synthesizing three different carbon microstructures from a single biowaste Bombax malabaricum for fully biocompatible flexible supercapacitors and their performance in various electrolytes. *ACS Omega* 2019;4:6399–410. <https://doi.org/10.1021/acsomega.9b00263>.
- [10] Péan C, Merlet C, Rotenberg B, Madden PA, Taberna PL, Daffos B, et al. On the dynamics of charging in nanoporous carbon-based supercapacitors. *ACS Nano* 2014;8:1576–83. <https://doi.org/10.1021/nn4058243>.
- [11] Samantaray SS, Mangiseti SR, Ramaprabhu S. Investigation of room temperature hydrogen storage in biomass derived activated carbon. *J Alloys Compd* 2019;789:800–4. <https://doi.org/10.1016/j.jallcom.2019.03.110>.
- [12] Lee SH, Lee TH. High performance hybrid supercapacitors with LiNi₁/3Mn₁/3Co₁/3O₂/activated carbon cathode and activated carbon anode. *Int J Hydrogen Energy* 2018;43:15365–9. <https://doi.org/10.1016/j.ijhydene.2018.06.089>.
- [13] Xing L, Wu X, Huang K. High-performance supercapacitor based on three-dimensional flower-shaped Li₄Ti₅O₁₂-graphene hybrid and pine needles derived honeycomb carbon. *J Colloid Interface Sci* 2018;529:171–9. <https://doi.org/10.1016/j.jcis.2018.06.007>.
- [14] Xing L-L, Zhao G-G, Huang K-J, Wu X. A yolk-shell V₂O₅ structure assembled from ultra-thin nanosheets and coralline-shaped carbon as advanced electrodes for a high performance asymmetric supercapacitor. *Dalton Trans* 2018;47:2256–65. <https://doi.org/10.1039/c7dt04660j>.
- [15] Gao Y-P, Zhai Z-B, Huang K-J, Zhang Y-Y. Energy storage applications of biomass-derived carbon materials: batteries and supercapacitors. *New J Chem* 2017;41:11456–70. <https://doi.org/10.1039/c7nj02580g>.
- [16] He S, Chen W. 3D graphene nanomaterials for binder-free supercapacitors: scientific design for enhanced performance. *Nanoscale* 2015;7:6957–90. <https://doi.org/10.1039/C4NR05895J>.
- [17] Venkateshalu S, Nirmala A, Electrochem GJ, Venkateshalu S, Nirmala A. Review — heterogeneous 3D graphene derivatives for supercapacitors. *J Electrochem Soc* 2020;167. <https://doi.org/10.1149/1945-7111/ab6bc5>. 050509-20.
- [18] Zhang Y, Wen G, Fan S, Ma W. 3D Carboxyl and hydroxyl co-enriched graphene hydrogels as binder-free electrodes for symmetric supercapacitors. *Int J Hydrogen Energy* 2019;44:23726–40. <https://doi.org/10.1016/j.ijhydene.2019.07.045>.
- [19] Çögenli MS, Yurtcan AB. Heteroatom doped 3D graphene aerogel supported catalysts for formic acid and methanol oxidation. *Int J Hydrogen Energy* 2020;45:650–66. <https://doi.org/10.1016/j.ijhydene.2019.10.226>.
- [20] Frackowiak E, Béguin F. Carbon materials for the electrochemical storage of energy in capacitors. *Carbon N Y* 2001;39:937–50. [https://doi.org/10.1016/S0008-6223\(00\)00183-4](https://doi.org/10.1016/S0008-6223(00)00183-4).
- [21] Kim C, Zhu C, Aoki Y, Habazaki H. Heteroatom-doped porous carbon with tunable pore structure and high specific surface area for high performance supercapacitors. *Electrochim Acta* 2019;314:173–87. <https://doi.org/10.1016/j.electacta.2019.05.074>.
- [22] Li B, Xing R, Mohite SV, Latthe SS, Fujishima A, Liu S, et al. CoS₂ nanodots anchored into heteroatom-doped carbon layer via a biomimetic strategy: boosting the oxygen evolution and supercapacitor performance. *J Power Sources* 2019;436:226862–9. <https://doi.org/10.1016/j.jpowsour.2019.226862>.
- [23] Rani S, Kamaraj M, Ramaprabhu S. Electrochimica Acta N-doped 3D porous carbon-graphene/polyaniline hybrid and N-doped porous carbon coated gC₃N₄ nanosheets for excellent energy density asymmetric supercapacitors. *Electrochim Acta* 2019;305:264–77. <https://doi.org/10.1016/j.electacta.2019.03.043>.
- [24] Shaheen S, Alfasane A, Akolade I, Aziz A, Yamani ZH. Polyaniline and heteroatoms – enriched carbon derived from Pithophora polymorpha composite for high performance supercapacitor. *J Energy Storage* 2020;30:101562. <https://doi.org/10.1016/j.est.2020.101562>.
- [25] Xing L, Huang K, Cao S, Pang H. Chestnut shell-like Li₄Ti₅O₁₂ hollow spheres for high-performance aqueous asymmetric supercapacitors. *Chem Eng J* 2018;332:253–9. <https://doi.org/10.1016/j.cej.2017.09.084>.
- [26] Pan Z, Zhi H, Qiu Y, Yang J, Xing L, Zhang Q, et al. Achieving commercial-level mass loading in ternary-doped holey graphene hydrogel electrodes for ultrahigh energy density supercapacitors. *Nanomater Energy* 2018;46:266–76. <https://doi.org/10.1016/j.nanoen.2018.02.007>.
- [27] Liang Q, Ye L, Huang Z-H, Xu Q, Bai Y, Kang F, et al. A honeycomb-like porous carbon derived from pomelo peel for use in high-performance supercapacitors. *Nanoscale* 2014;6:13831–7. <https://doi.org/10.1039/C4NR04541F>.
- [28] Xia J, Zhang N, Chong S, Li D, Chen Y, Sun C. Three-dimensional porous graphene-like sheets synthesized from biocarbon via low-temperature graphitization for a

- supercapacitor. *Green Chem* 2018;20:694–700. <https://doi.org/10.1039/C7GC03426A>.
- [29] Yao L, Wu Q, Zhang P, Zhang J, Wang D, Li Y, Ren X, Mi H, Deng L, Zhang Z. Scalable 2D hierarchical porous carbon nanosheets for flexible supercapacitors with ultrahigh energy density. *Adv Mater* 2018;30:1–9. <https://doi.org/10.1002/adma.201706054>.
- [30] Jung SH, Myung Y, Kim BN, Kim IG, You IK, Kim TY. Activated biomass-derived graphene-based carbons for supercapacitors with high energy and power density. *Sci Rep* 2018;8:1–8. <https://doi.org/10.1038/s41598-018-20096-8>.
- [31] Sun H, Cao L, Lu L. Bacteria promoted hierarchical carbon materials for high-performance supercapacitor. *Energy Environ Sci* 2012;5:6206–13. <https://doi.org/10.1039/c2ee03407g>.
- [32] Zhang Q, Han K, Li S, Li M, Li J, Ren K. Synthesis of garlic skin-derived 3D hierarchical porous carbon for high-performance supercapacitors. *Nanoscale* 2018;10:2427–37. <https://doi.org/10.1039/C7NR07158B>.
- [33] Chavhan S, Miguel O, Grande H-J, Victoria G-P, Rafael SS, Barea EM, Ivañ M-S, Ramoñ T-Z. Organo-metal halide pervoskite-based solar cells with CuSCN as the inorganic hole selective contact. *J Mater Chem* 2014;2:12754–60. <https://doi.org/10.1039/b000000x>.
- [34] Chen L, Huang Z, Liang H, Gao H, Yu S. Three-dimensional heteroatom-doped carbon nanofiber networks derived from bacterial cellulose for supercapacitors. *Adv Funct Mater* 2014;24:1–8. <https://doi.org/10.1002/adfm.201400590>.
- [35] Tian W, Zhang H, Sun H, Suvorova A, Saunders M, Tade M, et al. Heteroatom (N or N-S)-Doping induced layered and honeycomb microstructures of porous carbons for CO₂ capture and energy applications. *Adv Funct Mater* 2016;26:8651–61. <https://doi.org/10.1002/adfm.201603937>.
- [36] Tian W, Gao Q, Zhang L, Yang C, Li Z, Yanli T, Qian W, Zhang H. Renewable graphene-like nitrogen-doped carbon nanosheets as supercapacitor electrodes with integrated high energy-power properties. *J Mater Chem* 2016;4:8690–9. <https://doi.org/10.1039/C6TA02828D>.
- [37] Wang T, Wang LX, Wu DL, Xia W, Jia DZ. Interaction between nitrogen and sulfur in co-doped graphene and synergetic effect in supercapacitor. *Sci Rep* 2015;5:1–9. <https://doi.org/10.1038/srep09591>.
- [38] Li X, Xu Y, Hu G, Luo Z, Xu D, Tang T, et al. Self-assembled formation of conjugated 3D reduced graphene oxide-wrapped helical CNTs nanostructure and nitrogen-doped using photochemical doping for high-performance supercapacitor electrodes. *Electrochim Acta* 2018;280:33–40. <https://doi.org/10.1016/j.electacta.2018.05.106>.
- [39] Liu Y, Qiu X, Liu X, Liu Y, Fan L-Z. 3D porous binary-heteroatom doped carbon nanosheet/electrochemically exfoliated graphene hybrids for high performance flexible solid-state supercapacitors. *J Mater Chem* 2018;6:8750–6. <https://doi.org/10.1039/C8TA01148F>.
- [40] Tran NQ, Kang BK, Woo MH, Yoon DH. Enrichment of pyrrolic nitrogen by hole defects in nitrogen and sulfur co-doped graphene hydrogel for flexible supercapacitors. *ChemSusChem* 2016;9:2261–8. <https://doi.org/10.1002/cssc.201600668>.
- [41] Yang W, Hou L, Xu X, Li Z, Ma X, Yang F, et al. Carbon nitride template-directed fabrication of nitrogen-rich porous graphene-like carbon for high performance supercapacitors. *Carbon N Y* 2018;130:325–32. <https://doi.org/10.1016/j.carbon.2018.01.032>.
- [42] Zhang W, Chen Z, Guo X, Jin K, Wang Y, Li L, et al. SC. *Electrochim Acta* 2018. <https://doi.org/10.1016/j.electacta.2018.05.018>.
- [43] Zhao G, Chen C, Yu D, Sun L, Yang C, Zhang H, Sun Y, Besenbacher F, Yu M. One-step production of O-N-S Co-doped three-dimensional hierarchical porous carbons for high-performance supercapacitors. *Nanomater Energy* 2018;47:547–55. <https://doi.org/10.1016/j.nanoen.2018.03.016>.
- [44] Chen H, Yu F, Wang G, Chen L, Dai B, Peng S. Nitrogen and sulfur self-doped activated carbon directly derived from elm flower for high-performance supercapacitors. *ACS Omega* 2018;3:4724–32. <https://doi.org/10.1021/acsomega.8b00210>.
- [45] Cheng L, Hu Y, Qiao D, Zhu Y, Wang H, Jiao Z. One-step radiolytic synthesis of heteroatom (N and S) co-doped graphene for supercapacitors. *Electrochim Acta* 2017. <https://doi.org/10.1016/j.electacta.2017.11.022>.
- [46] Kota M, Jana M, Park HS. Improving energy density of supercapacitors using heteroatom-incorporated three-dimensional macro-porous graphene electrodes and organic electrolytes. *J Power Sources* 2018;399:83–8. <https://doi.org/10.1016/j.jpowsour.2018.07.078>.
- [47] Li Y, Wang G, Wei T, Fan Z, Yan P. Nitrogen and sulfur co-doped porous carbon nanosheets derived from willow catkin for supercapacitors. *Nanomater Energy* 2016;19:165–75. <https://doi.org/10.1016/j.nanoen.2015.10.038>.
- [48] Lal MS, Sundara R. High entropy oxides - a cost-effective catalyst for the growth of high yield carbon nanotubes and their energy applications. *ACS Appl Mater Interfaces* 2019;11:30846–57. <https://doi.org/10.1021/acsami.9b08794>.
- [49] Sham Lal M, Lavanya T, Ramaprabhu S. An efficient electrode material for high performance solid-state hybrid supercapacitors based on a Cu/CuO/porous carbon nanofiber/TiO₂ hybrid composite. *Beilstein J Nanotechnol* 2019;10:781–93. <https://doi.org/10.3762/bjnano.10.78>.
- [50] Chandrabhan Shende R, Muruganathan M, Mizuta H, Akabori M, Sundara R. Chemical simultaneous synthesis strategy of two nitrogen-rich carbon nanomaterials for all-solid-state symmetric supercapacitor. *ACS Omega* 2018;3:17276–86. <https://doi.org/10.1021/acsomega.8b02835>.
- [51] Yu J, Fu N, Zhao J, Liu R, Li F, Du Y, et al. High specific capacitance electrode material for supercapacitors based on resin-derived nitrogen-doped porous carbons. *ACS Omega* 2019;4. <https://doi.org/10.1021/acsomega.9b01916>. 15904–11.
- [52] Tamilarasan P, Ramaprabhu S. Ionic liquid-functionalized partially exfoliated multiwalled carbon nanotubes for high-performance supercapacitors. *J Mater Chem* 2014;2:14054–63. <https://doi.org/10.1039/c4ta02718c>.